

The Detection of Transiting Exoplanets by *Gaia*

Aviad Panahi¹, Shay Zucker², Gisella Clementini³, Marc Audard⁴, Avraham Binnefeld², Felice Cusano³, Dafydd Wyn Evans⁵, Roy Gomel¹, Berry Holl⁴, Ilya Ilyin⁶, Grégory Jevardat de Fombelle⁴, Tsevi Mazeh¹, Nami Mowlavi⁴, Krzysztof Nienartowicz^{4,7}, Lorenzo Rimoldini⁴, Sahar Shahaf⁸, and Laurent Eyer⁴

¹ School of Physics and Astronomy, Raymond and Beverly Sackler Faculty of Exact Sciences, Tel Aviv University, Tel Aviv 6997801, Israel

² Porter School of the Environment and Earth Sciences, Raymond and Beverly Sackler Faculty of Exact Sciences, Tel Aviv University, Tel Aviv 6997801, Israel

³ INAF - Osservatorio di Astrofisica e Scienza dello Spazio di Bologna, via Piero Gobetti 93/3, 40129 Bologna, Italy

⁴ Department of Astronomy, University of Geneva, Chemin Pegasi 51, 1290 Versoix, Switzerland

⁵ Institute of Astronomy, University of Cambridge, Madingley Road, Cambridge CB3 0HA, UK

⁶ Leibniz-Institut für Astrophysik Potsdam (AIP), An der Sternwarte 16, 14482 Potsdam, Germany

⁷ Sednai Sàrl, Geneva, Switzerland

⁸ Department of Particle Physics and Astrophysics, Weizmann Institute of Science, Rehovot 7610001, Israel

Received March 8, 2022; accepted May 19, 2022

ABSTRACT

Context. The space telescope *Gaia* is dedicated mainly to performing high-precision astrometry, but also spectroscopy and epoch photometry which can be used to study various types of photometric variability. One such variability type is exoplanetary transits. The photometric data accumulated so far have finally matured enough to allow the detection of some exoplanets.

Aims. In order to fully exploit the scientific potential of *Gaia*, we search its photometric data for the signatures of exoplanetary transits.

Methods. The search relies on a version of the Box-Least-Square (BLS) method, applied to a set of stars prioritized by machine-learning classification methods. An independent photometric validation was obtained using the public full-frame images of *TESS*. In order to validate the first two candidates, radial-velocity follow-up observations were performed using the spectrograph PEPSI of the Large Binocular Telescope (LBT).

Results. The radial-velocity measurements confirm that two of the candidates are indeed hot Jupiters. Thus, they are the first exoplanets detected by *Gaia* – *Gaia*-1b and *Gaia*-2b.

Conclusions. *Gaia*-1b and *Gaia*-2b demonstrate that the approach presented in this paper is indeed effective. This approach will be used to assemble a set of additional exoplanet candidates, to be released in *Gaia* third data release, ensuring better fulfillment of the exoplanet detection potential of *Gaia*.

Key words. Methods: data analysis – planets and satellites: detection – techniques: photometric – techniques: radial velocities

1. Introduction

Transit photometry is currently the most prolific method for detecting exoplanets, with more than 3 000 discovered to this day, mostly using space-based missions, like *Kepler* (Borucki et al. 2010) and *TESS* (Ricker et al. 2015). These missions excel in detecting exoplanets thanks to their high cadence, highly-precise photometry and continuous sampling of large samples of stars. Nevertheless, there is still some chance that sparse low-cadence photometry, while far from being optimal for that purpose, would also be able to detect transiting exoplanets. In fact, the transits of two exoplanets that had been detected by radial velocities – HD 209458b (Charbonneau et al. 2000) and HD 189733b (Bouchy et al. 2005) were later found in the archived photometry of the first all-sky astrometric mission *Hipparcos* (Perryman et al. 1997). The *Hipparcos* photometric time series had fewer than 200 measurements each, but still managed to sample the planetary transits (Robichon & Arenou 2000; Hébrard & Lecavelier Des Etangs 2006). These detections proved it was possible that such sparse and low-cadence observations may sample a meaningful number of transit events.

The current astrometric mission *Gaia* (Gaia Collaboration et al. 2016) has already revolutionized astronomy with its high-precision astrometry for about 1.8 billion stars. On the other hand, similarly to *Hipparcos*, the photometry produced by *Gaia* is very sparse, with an irregular sampling scheme, which as mentioned above is suboptimal for detecting exoplanetary transits. Still, early on in its first two years of operation *Gaia* did manage to capture some transits of previously-known exoplanets, such as WASP 19 b (Hebb et al. 2009) and WASP 98 b (Hellier et al. 2014)¹. Dzigan & Zucker (2012) estimated that with five years of *Gaia* photometry (which is more precise than that of *Hipparcos*) it should be possible to detect several hundreds of transiting Jovian exoplanets, as well as brown dwarfs (Holl et al. 2021).

As members of the Data Processing and Analysis Consortium (DPAC) of *Gaia*, we hereby present the approach taken by DPAC in order to exploit the potential of *Gaia* to detect transiting exoplanets. We have found 41 candidates and validated by radial-velocity (RV) follow-up observations the first two candidate planet host-stars: *Gaia* EDR3 3026325426682637824 and

¹ https://www.cosmos.esa.int/web/gaia/iow_20170209

Gaia EDR3 1107980654748582144, which we will henceforth refer to as Gaia-1 and Gaia-2, respectively.

Sect. 2 describes the search procedure, including validation by *TESS* photometry. Sect. 3 presents a detailed analysis of the two candidates that we validated with RV measurements. Finally we conclude in Sect. 4 and put the results in the context of *Gaia* data releases.

2. Methods

Transit-finding algorithms, such as the box-fitting least squares (BLS) algorithm (Kovács et al. 2002), have a typical time complexity of $O(N \cdot N_p)$, where N is the number of points in the light curve and N_p is the number of trial periods scanned. *Gaia* Early Data Release 3 (EDR3) is the result of analyzing the data of the first 34 months of *Gaia* operation, and scanning for periods in a range of [0.5, 100] days would require about $O(10^4)$ trial periods. With 1.8 billion stars in the *Gaia* database, and having a few dozen measurements for each star, applying the conventional search algorithms to all of them would be prohibitively time-consuming and impractical. Therefore we decided not to perform an exhaustive transit search on all the observed stars, but focus on stars that passed an initial examination, as part of a general classification step that used machine learning methods to classify *Gaia* time series into variability classes (Sect. 2.3).

2.1. Gaia photometry

The light curves we scanned included the combined epoch photometry from all three photometric bands of *Gaia* – G , G_{BP} and G_{RP} , after independently subtracting their median magnitudes. We combined the three bands in an effort to increase the number of samples in each light curve, assuming the transit effect is achromatic (to a first approximation) and would therefore be similar in all three bands. We searched for outliers based on their distance from the median magnitude, in terms of the standard deviation, σ , and excluded samples that were 2σ brighter or 5σ fainter than the median.

2.2. Training set

We compiled a training set consisting of *Gaia* light curves with noticeable transits of previously known exoplanets. We applied a dedicated version we have developed of the BLS algorithm to the *Gaia* light curves of all known transiting exoplanets in order to find these transits. This version is scanning a restricted range in the parameter space of the three temporal transit parameters: period, mid-transit time and duration. We use a very similar approach in another study in which we use *Gaia* photometry to test for false positives in the *TESS* detections due to blends with background binaries (Panahi et al., in prep). The scan only covered a range of $\pm 3\sigma$ for each transit parameter, as published in the NASA exoplanet archive (Akeson et al. 2013). At the end of each run, a set of preliminary transit parameters was obtained, along with a statistic we dubbed Transit SNR (SNR_T):

$$SNR_T \equiv \frac{d}{\sigma_{OOT}} \sqrt{N_{IT}}, \quad (1)$$

where d is the transit depth found by BLS, σ_{OOT} is the standard deviation of the out-of-transit (OOT) measurements (as a proxy to the random variability of the whole light curve), and N_{IT} is the number of in-transit (IT) points. We visually inspected the folded light curves of the stars that had $SNR_T > 6$ and selected

the ones with a clear transit-like signal, resulting in 77 sources to be used as the training set.

2.3. Classification

A general supervised classification module was applied to all variability types (Rimoldini et al., in prep.) that included a generic computationally efficient period search method (Generalised Lomb-Scargle, GLS; Zechmeister & Kürster 2009), although it was not necessarily optimal for all classes. Given the weak signal of exoplanetary transits and the likely unreliable period GLS obtained for them, the classifier was designed to attempt initial identification of this class from simple epoch photometry statistics in the three *Gaia* bands, without the important test of periodicity.

Consequently, the initial set of 77 training sources was further trimmed to enhance the clarity of the signal and thus the chances of detection. For example, sources with negative G -band standardized skewness (in magnitude) were excluded, as noise fluctuations on the bright side of the time series were larger than the transit signal in those cases. Eventually only 66 sources were used to train classifiers for exoplanetary transits, among a training set of almost 60 000 objects and 40 classes (before the selection of publishable classes).

Random Forest (Breiman 2001) and XGBoost (Chen & Guestrin 2016) classification methods were used to model the training set with a list of attributes defined in section 10.3.3 of Rimoldini et al. (2022)². The XGBoost classifier was distinctively more effective than Random Forest in naturally identifying these rare training objects and it was thus adopted for predicting exoplanetary transits. This resulted in a total number of 18 383 candidates.

2.4. Initial candidates

We applied to the 18 383 initial candidates a dedicated implementation of the BLS algorithm – SparseBLS (Panahi & Zucker 2021), which we had developed especially for *Gaia* photometry. Unlike the BLS version that we used to compile the training set (Sect. 2.2), SparseBLS scans only an array of trial periods and estimates the mid-transit time and transit duration from the actual data timestamps, as opposed to a pre-determined grid. SparseBLS is especially suitable for sparse light curves containing hundreds of measurements or fewer, since the run-time depends quadratically on the number of samples in the light curve.

We scanned with SparseBLS periods in the range of [0.5, 100] days, with a frequency step of $\Delta f = 10^{-5} \text{ d}^{-1}$. This resulted in preliminary transit parameters, including period, time of mid-transit and transit depth, along with other BLS statistics, such as the Signal Detection Efficiency (SDE) (Kovács et al. 2002; Alcock et al. 2000), which quantifies the prominence of the periodogram peak. Similarly to BLS, SparseBLS uses the Signal Residue (SR) score for its periodogram. The SR is the part of the sum of squared residuals in a least-square fit that depends on the attempted model. For this score the SDE is simply defined as:

$$SDE = \frac{SR_{\text{peak}} - \langle SR \rangle}{\text{sd}(SR)}, \quad (2)$$

where SR_{peak} is the highest value of the periodogram, $\langle SR \rangle$ is the SR mean value, and $\text{sd}(SR)$ is the standard deviation of the SR values in the periodogram.

² To be made public with *Gaia* Data Release 3 (DR3).

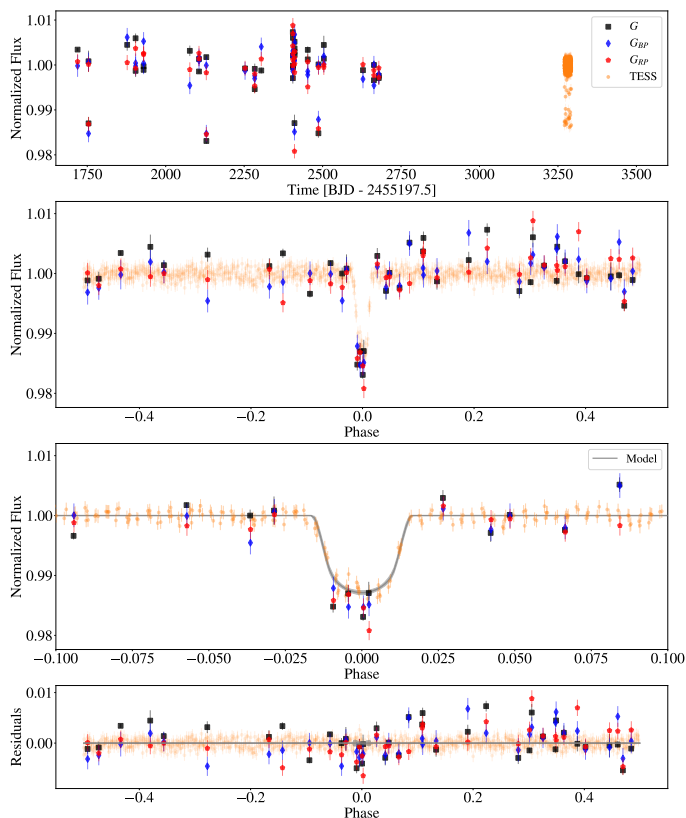


Fig. 1. *Gaia*-1: (Top) combined photometry of *Gaia* and *TESS* FFI. (Second panel) Phase-folded light curves according to the transit parameters listed in Table 4. (Third panel) Zoom in on transit. (Bottom) Residuals showing a possible systematic effect.

In order to narrow down the list of final candidates we applied the following cuts to the resulting parameters :

- $SNR_T > 7.5$
- $S_{\text{SparseBLS SDE}} > 6$
- $\text{Transit depth} < 40 \text{ mmag}$.

The last criterion was an attempt to avoid cases of eclipsing binaries, or Jovian exoplanets around M dwarfs, which usually have depths larger than 40 mmag. Those cases should be detectable by other tasks focusing on eclipsing binaries. We visually inspected the remaining 130 candidates to look for clear transit-like features. We excluded 41 candidates that did not meet the following criteria:

- Host star is a Main-Sequence star.
- Achromatic transit seen in G_{BP} and G_{RP} .
- Transit is not V-shaped.
- No visible out-of-transit variability.
- No visible secondary eclipse.
- No visible odd-even difference in *TESS* photometry.

2.5. Photometric validation

In order to validate photometrically the remaining 89 candidates, we searched for their light curves in the Full-Frame Image (FFI) photometry of *TESS*. About half of them (48) were found more likely to be eclipsing binaries, or exhibited no transit in the *TESS* data. Within the remaining 41 candidates (to be published in *Gaia* DR3, along with 173 known exoplanets with visible transits in the photometry of *Gaia*; Eyer et al., in prep.), we were

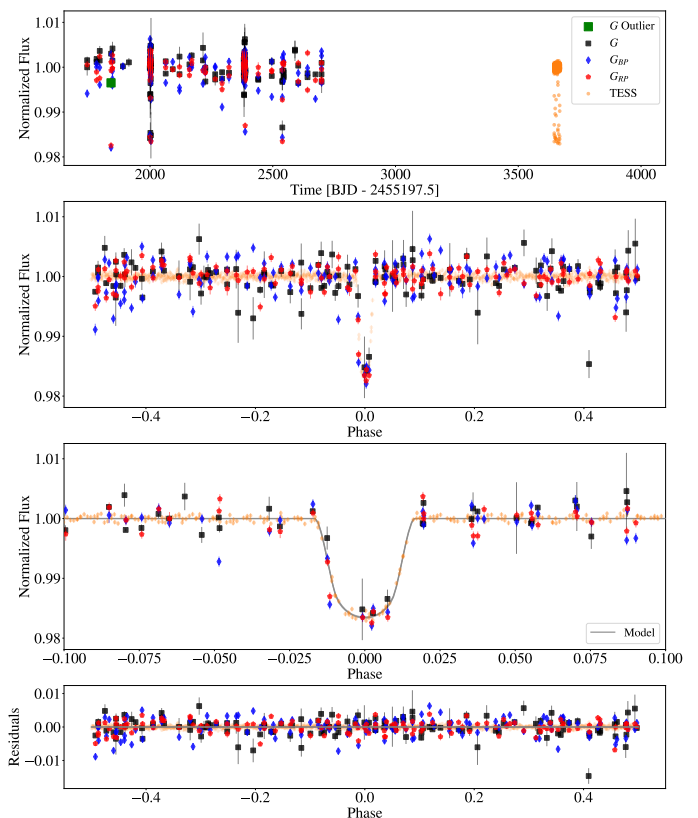


Fig. 2. *Gaia*-2: (Top) combined photometry of *Gaia* and *TESS* FFI. (Second panel) Phase-folded light curves according to the transit parameters listed in Table 4. (Third panel) Zoom in on transit. (Bottom) Residuals with no visible systematic effects.

able to find significant transit-like signals in the FFI data for 21 stars. For these 21 stars we used the FFI data to refine the transit parameters we had calculated during the preparation of the initial candidate set.

3. Confirmed planets

We selected two of our leading candidates for confirmation by RV follow-up observations. Figs. 1 and 2 show the normalized and combined photometry of *Gaia* and *TESS* for these two candidates, *Gaia*-1 and *Gaia*-2, along with the best-fitting models (Sect. 3.3), with 68% confidence intervals. We detrended the *Gaia* light curves using a simple linear fit. For the *TESS* light curves we used the Python packages *Lightkurve* (Lightkurve Collaboration et al. 2018) and *tesscut* (Brasseur et al. 2019) to acquire the *TESS* FFI photometry, and the `flatten()` method to detrend the raw data.

The combined light curve of *Gaia*-1 contain 117 measurements of *Gaia* (in all three bands) and 952 measurements of *TESS*. We note the slight dilution in the *TESS* light curve of *Gaia*-1. This may be due to the relatively large point spread function (PSF) of *TESS*³, where the dilution is caused by the blended light of nearby stars included in the PSF. *Gaia*-2 is much brighter than its close neighbors and the blending effect is unnoticeable.

In the case of *Gaia*-2 we decided to exclude one measurement⁴ from the *Gaia* *G* band that resided, after phase folding,

³ In fact the relevant size in *TESS* is the pixel response function – PRF. See Section 6 of the *TESS Instrument Handbook*.

⁴ $t = 1841.3424606$ (BJD – 2455197.5), marked with a green square in the top panel of Fig. 2.

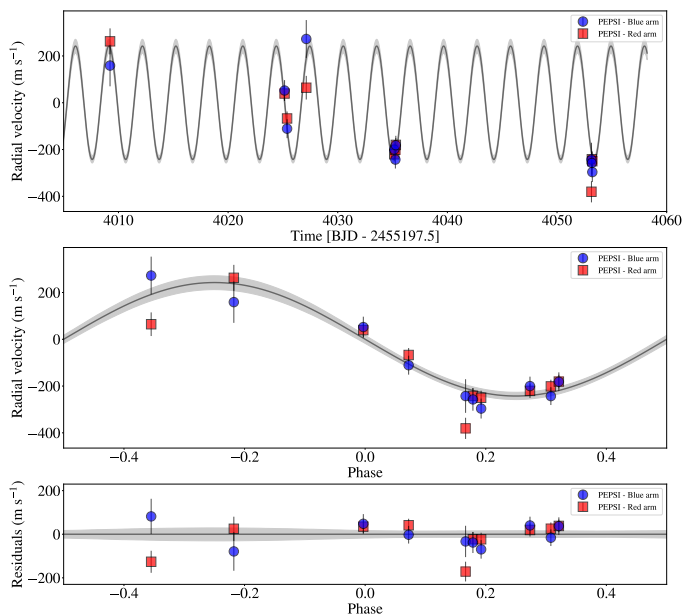


Fig. 3. (Top) PEPSI RV measurements of Gaia-1, on top of the best-fitting RV curve (solid line) derived by *juliet*. We subtracted the systemic velocity, listed in Table 4. (Middle) Phase-folded RV curves according to the period listed in Table 4. (Bottom) Residuals with no visible systematic variation.

in the middle of the transit, with a normalized flux of $f_{\text{norm}} = 0.9965$. A closer look at this specific measurement reveals several indications for possible saturation. Furthermore, the G_{BP} and G_{RP} measurements, taken at almost the same time, do agree with the transit model. Therefore and thanks to the validation by *TESS* photometry, we were confident that this point was indeed an outlier, and that we could fit a more accurate model after excluding it. The combined light curve of Gaia-2 contains 394 measurements of *Gaia* (in all three bands) and 1183 measurements of *TESS*.

3.1. Host stars

The host stars Gaia-1 and Gaia-2 are listed in the *TESS* Input Catalog (TIC; Stassun et al. 2018) with mass and radius estimates. We also used *Gaia* data to estimate these values independently, using the Python package *isochrones* (Morton 2015). This tool uses stellar evolution models, based on the distance and observable magnitudes in multiple bands. We used the *Gaia* parallax and the three magnitudes (G , G_{BP} , G_{RP}), and obtained similar estimates, as listed in Table 1.

3.2. Radial velocities

We obtained high-resolution spectra for the two candidates, using the spectrograph PEPSI (Strassmeier et al. 2015), on the Large Binocular Telescope (LBT). The PEPSI spectrograph has two arms, blue and red, with six cross-dispersers for a full optical coverage in the range of 383 – 907 nm. In this work we used the high-resolution configuration with $R = 50\,000$ using cross-dispersers 2 (blue arm) and 4 (red arm), covering the wavelength ranges 426 – 480 and 544 – 627 nm, respectively (Strassmeier et al. 2015). The PEPSI pipeline produces a one-dimensional spectrum for each order, wavelength-calibrated using a ThAr lamp, continuum-normalized and corrected for solar barycentric motion. The cross-correlation function (CCF) was calculated

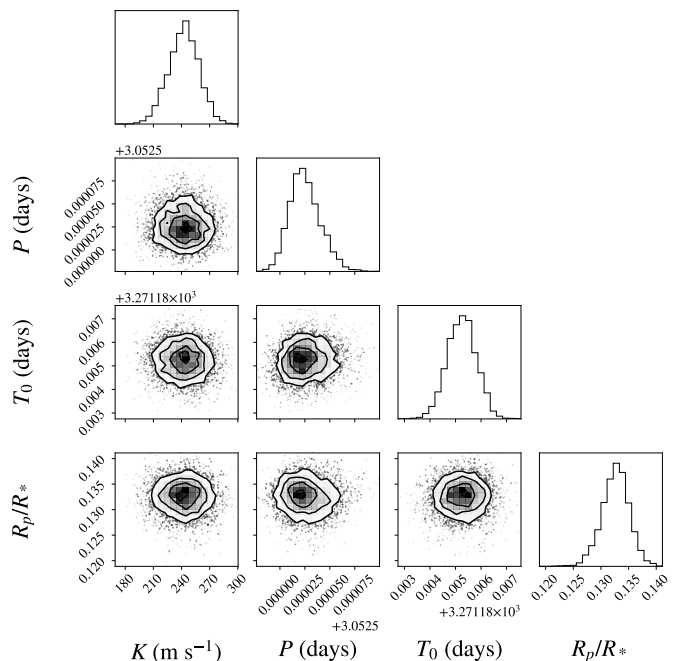


Fig. 4. Gaia-1b: Corner plot of the posterior distributions of the main system parameters, assuming circular orbit.

independently for each spectral order. The radial velocities and their uncertainties were derived from the combined CCF, according to Zucker (2003), using the Python package SPARTA (Shahaf et al. 2020). The RV modulations are detailed in Table 2, with the systemic velocity subtracted (See Table 4).

3.3. Analysis

We performed joint analyses incorporating the photometry of *Gaia* and *TESS*, together with the RV data of the red and blue arms of PEPSI as effectively two different instruments, using the Python package *juliet* (Espinoza et al. 2019). *juliet* uses *batman*, (Kreidberg 2015) for modeling the transit light curve and *radvel* (Fulton et al. 2018) for modeling the RV curve. *juliet* uses several parametrization schemes that allow the sampling of the parameter space while maintaining the physical validity of the model. Espinoza (2018) and Kipping (2013) provide additional details of the sampling schemes and the parametrization. We used the Dynamic Nested Sampling method (*dynesty*; Speagle 2020) to get parameter posterior estimates, along with the Bayesian log evidence ($\ln Z$) for each model, useful for comparing different models. According to Trotta (2008), a difference of $\Delta \ln Z < 1$ means the two models should be considered statistically indistinguishable, while $\Delta \ln Z > 5$ suggests strong evidence in favor of the model with the larger value of $\ln Z$. Besides selecting *dynesty* for the sampling method, all other parameters of the `fit()` method of *juliet* were left in their default values. Convergence is achieved when the program fails to improve its $\ln Z$ value by 0.5 in one complete iteration.

Given the relatively low number of RV measurements, we decided to assume a circular orbit and fix the eccentricity at zero, as expected for planets with such short periods (e.g. Wu 2003). We used similar priors for the various parameters as those used by Espinoza et al. (2020), which we detail in Table 3. We have set all jitter terms σ_{ω} to zero, as well as the flux offset terms M , since we used normalized light curves in this analysis. The mean

Table 1. Stellar parameter estimates for *Gaia*-1 and *Gaia*-2.

Parameter	Units	Value		Source
		Gaia-1	Gaia-2	
Gaia SourceID		3026325426682637824	1107980654748582144	Gaia EDR3
TIC ID		11755687	147797743	TIC
RA	deg	$90.6436666838 \pm 3.4 \cdot 10^{-9}$	$110.7353331726 \pm 2.2 \cdot 10^{-9}$	Gaia EDR3
DEC	deg	$-0.5771154808 \pm 3.0 \cdot 10^{-9}$	$67.2526599247 \pm 4.3 \cdot 10^{-9}$	Gaia EDR3
G	mag	12.99192 ± 0.00055	11.20014 ± 0.00043	Gaia
G_{BP}	mag	13.38862 ± 0.00051	11.54127 ± 0.00026	Gaia
G_{RP}	mag	12.41065 ± 0.00051	10.69055 ± 0.00028	Gaia
V	mag	13.242 ± 0.092	11.277 ± 0.008	TIC
Parallax	mas	2.715 ± 0.015	4.826 ± 0.023	Gaia EDR3
T_{eff}	K	5470 ± 110	5720 ± 84	isochrones
M_*	M_{\odot}	0.949 ± 0.066	1.000 ± 0.095	isochrones
R_*	R_{\odot}	0.952 ± 0.025	1.064 ± 0.031	isochrones
ρ_*	kg m^{-3}	1558 ± 170	1170 ± 160	isochrones
T_{eff}	K	5370 ± 140	5720 ± 130	TIC
M_*	M_{\odot}	0.93 ± 0.12	1.02 ± 0.13	TIC
R_*	R_{\odot}	0.962 ± 0.054	1.088 ± 0.053	TIC
ρ_*	kg m^{-3}	1480 ± 310	1120 ± 220	TIC

Table 2.

PEPSI RV measurements of *Gaia*-1 and *Gaia*-2, extracted with SPARTA. Systemic velocities of the circular orbits were removed (See Table 4).

Gaia-1

Time (BJD – 2455197.5)	RV _{Blue} (m s ⁻¹)	RV _{Red} (m s ⁻¹)
4009.231299	159 ± 89	262 ± 55
4025.149340	52 ± 44	39 ± 32
4025.378759	-111 ± 40	-67 ± 30
4027.127925	273 ± 81	64 ± 51
4035.150587	-200 ± 40	-220 ± 30
4035.256314	-243 ± 38	-201 ± 29
4035.296691	-181 ± 40	-180 ± 29
4053.139787	-243 ± 72	-380 ± 45
4053.176891	-257 ± 48	-242 ± 33
4053.218314	-296 ± 43	-250 ± 30

Gaia-2

Time (BJD – 2455197.5)	RV _{Blue} (m s ⁻¹)	RV _{Red} (m s ⁻¹)
4009.242638	-111 ± 30	-89 ± 26
4025.160356	55 ± 26	50 ± 14
4025.405016	90 ± 25	86 ± 14
4035.167108	-67 ± 25	-48 ± 14
4035.278306	-2 ± 25	-21 ± 14
4053.156642	-144 ± 27	-164 ± 14
4053.197203	-147 ± 25	-141 ± 14
4053.238726	-140 ± 25	-128 ± 14

values for the priors of the period and time of mid-transit were estimated based on the results of the preliminary analysis of the photometry.

The posterior medians and 68% confidence intervals of the system parameters resulting from the *juliet* analyses are detailed in Table 4, accompanied by corner plots (Foreman-Mackey 2016) for the main parameters in Figs. 4 and 6. We also used 68% confidence intervals for the RV models in Figs. 3 and

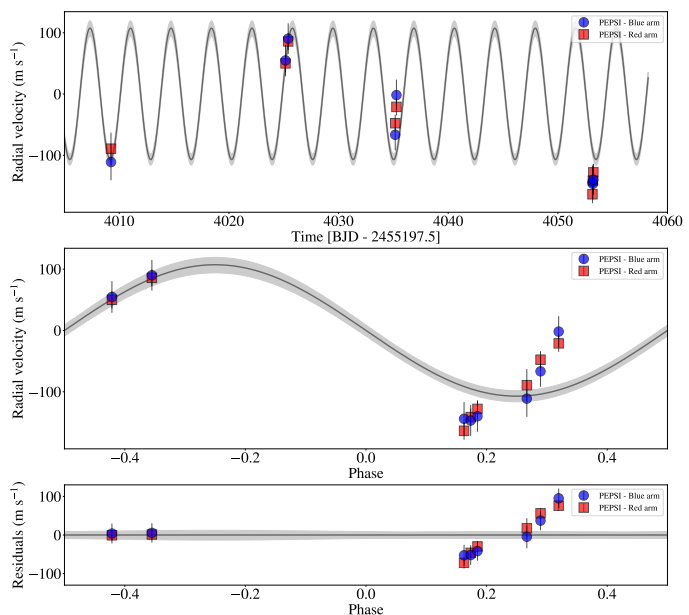


Fig. 5. (Top) PEPSI RV measurements of *Gaia*-2, on top of the best-fitting RV curve (solid line) derived by *juliet*. We subtracted the systemic velocity, listed in Table 4. (Middle) Phase-folded RV curves according to the period listed in Table 4. (Bottom) Residuals showing a possible systematic variation, perhaps due to some eccentricity of the orbit.

5. All two-dimensional histograms in the corner plots have four contour lines representing levels of (0.5, 1.0, 1.5, 2.0) sigmas.

3.4. *Gaia*-1b

The RVs of *Gaia*-1 seem to closely trace a sine curve (Fig. 3), as expected for a circular Keplerian orbit. Based on the estimated stellar parameters, we estimate the mass and radius of the transiting object to be $M_p = 1.68 \pm 0.11 M_J$, $R_p = 1.229 \pm 0.021 R_J$,

Table 3. Prior distributions for the joint photometry and RV analysis of Gaia-1b and Gaia-2b. We denote uniform distributions between a and b as $\mathcal{U}(a, b)$ and normal distributions with mean μ and variance σ^2 as $\mathcal{N}(\mu, \sigma^2)$.

Parameter	Description	Units	Prior	
			Gaia-1b	Gaia-2b
P	Period	days	$\mathcal{N}(3.052503, 0.01^2)$	$\mathcal{N}(3.691508, 0.01^2)$
T_0	Time of mid-transit	BJD - 2455197.5	$\mathcal{N}(3271.23705, 0.1^2)$	$\mathcal{N}(3646.43546, 0.1^2)$
K	Semi-amplitude of the radial velocity	m s^{-1}	$\mathcal{U}(0, 500)$	$\mathcal{U}(0, 500)$
e	Eccentricity	-	0 - fixed	0 - fixed ; $\mathcal{U}(0, 0.95)^i$
ω	Argument of periastron	degrees	0 - fixed	0 - fixed ; $\mathcal{U}(0, 360)^i$
ρ_*	Stellar mass mean density	kg m^{-3}	$\mathcal{N}(1558, 170^2)$	$\mathcal{N}(1173, 164^2)$
r_1, r_2	Parametrization of p, b^{ii}	-	$\mathcal{U}(0, 1)$	$\mathcal{U}(0, 1)$
$q_{1,\text{Gaia}}, q_{2,\text{Gaia}}$	Limb-darkening parametrization ⁱⁱⁱ for <i>Gaia</i>	-	$\mathcal{U}(0, 1)$	$\mathcal{U}(0, 1)$
D_{Gaia}	Dilution factor for <i>Gaia</i>	-	1 - fixed	1 - fixed
$q_{1,\text{TESS}}, q_{2,\text{TESS}}$	Limb-darkening parametrization ⁱⁱⁱ for <i>TESS</i>	-	$\mathcal{U}(0, 1)$	$\mathcal{U}(0, 1)$
D_{TESS}	Dilution factor for <i>TESS</i>	-	$\mathcal{U}(0.1, 1.0)$	$\mathcal{U}(0.1, 1.0)$
γ	Relative center-of-mass velocity for PEPSI ^{iv}	m s^{-1}	$\mathcal{U}(-500, 500)$	$\mathcal{U}(-500, 500)$

ⁱ Separate analysis, allowing eccentricity.

ⁱⁱ Described by Espinoza (2018), $p = R_p/R_*$ is the planetary to stellar radius ratio, and $b = (a/R_*) \cos i$ is the impact parameter.

ⁱⁱⁱ Described by Kipping (2013).

^{iv} Around a middle value of $-37\,750$ for Gaia-1b and $-36\,000$ for Gaia-2b.

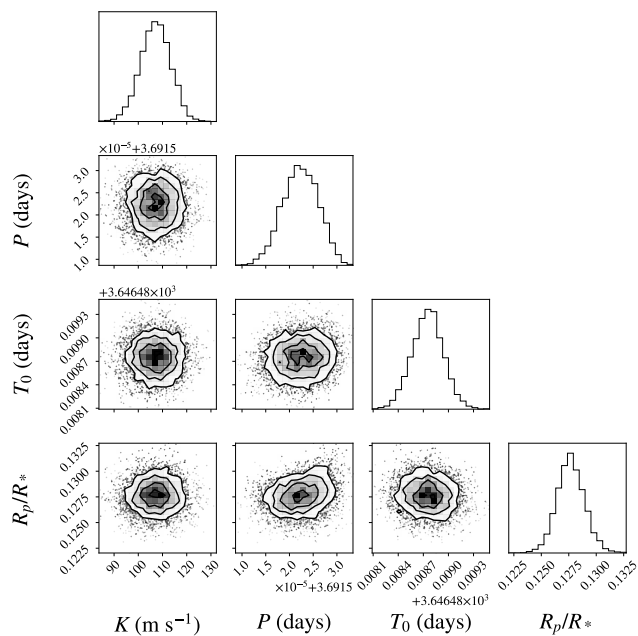


Fig. 6. Gaia-2b: Corner plot of the posterior distribution of the main system parameters, assuming circular orbit.

consistent with a possibly inflated hot Jupiter. For completeness, we tried to fit an eccentric orbit, but found no statistical evidence supporting an eccentric model ($\Delta \ln Z < 1$). When comparing to a model with no planet we got a value of $\Delta \ln Z = 109$, suggesting strong evidence for the existence of Gaia-1b. The residuals in Fig. 1 show a possible systematic variation, suggesting some out-of-transit variability, possibly due to a more massive companion. No such variability was observed in the photometry of *TESS*. Furthermore, the scatter seem not to be consistent among the three bandpasses of *Gaia* photometry, and the joint RV and

photometry analysis suggests a planetary companion. We therefore concluded there was no substantial evidence for this variability.

3.5. Gaia-2b

The phase coverage of the Gaia-2 RV measurements is sub-optimal (Fig. 5), especially around phase zero, and the phase-folded RV curve seems to suggest a potentially eccentric orbit. We therefore performed an additional analysis allowing non-zero eccentricity, with a uniform prior distribution $\mathcal{U}(0, 0.95)$, resulting in an estimate for the eccentricity of $e = 0.346 \pm 0.023$ with $\Delta \ln Z = 48$ over the circular orbit. The RVs with the eccentric model are shown in Fig. 7, and the posterior distributions and estimates for the main orbital parameters are given in Fig. 8 and Table 4. Despite the strong statistical evidence, such an eccentric orbit would be very surprising given the proximity of the planet to its host star. We therefore attempted also to fit a circular orbit with a constant slope in the RV curve, using a uniform prior distribution $\mathcal{U}(-300, 300) \text{ m s}^{-1} \text{ d}^{-1}$, resulting in an estimate for the RV slope of $RV_{\text{slope}} = -2.9 \pm 0.39 \text{ m s}^{-1} \text{ d}^{-1}$ with $\Delta \ln Z = 18$ over the no-slope, circular model. Statistically, the eccentric orbit seems to be preferable, but given the small number of measurements and their uncertainties, we decided to keep the more plausible circular orbit, and wait for future RV measurements to better constrain this system.

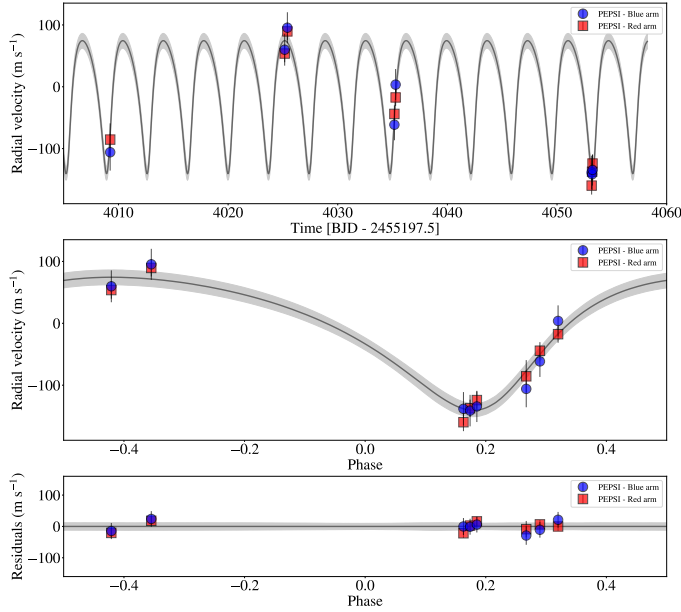
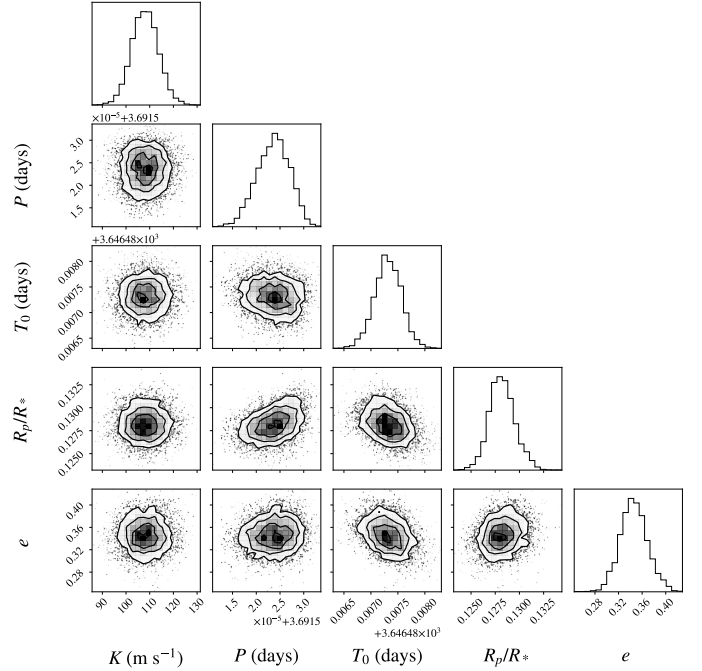
We then estimate the mass and radius of the transiting object to be $M_p = 0.817 \pm 0.047 M_J$, $R_p = 1.322 \pm 0.013 R_J$, also consistent with a potentially inflated hot Jupiter. When comparing to a model with no planet we got a value of $\Delta \ln Z = 133$, suggesting strong evidence for the existence of Gaia-2b.

4. Conclusions

In this paper we described the method used by DPAC to find the first batch of transiting exoplanet candidates based on *Gaia*

Table 4. Posterior estimates for *Gaia*-1b and *Gaia*-2b.

Parameter	Units	Value		
		Gaia-1b	Circular Orbit	Gaia-2b
P	days	$3.052524 \pm 1.7 \cdot 10^{-5}$	$3.6915224 \pm 3.9 \cdot 10^{-6}$	$3.6915237 \pm 3.5 \cdot 10^{-6}$
T_0	BJD - 2455197.5	$3271.18524 \pm 5.7 \cdot 10^{-4}$	$3646.48875 \pm 1.9 \cdot 10^{-4}$	$3646.48731 \pm 2.5 \cdot 10^{-4}$
r_1	-	$0.773^{+0.028}_{-0.037}$	0.806 ± 0.015	0.816 ± 0.015
r_2	-	0.124 ± 0.0023	0.1277 ± 0.0013	0.1282 ± 0.0013
$q_{1,Gaia}$	-	$0.24^{+0.25}_{-0.14}$	$0.125^{+0.125}_{-0.078}$	$0.138^{+0.123}_{-0.080}$
$q_{2,Gaia}$	-	$0.42^{+0.34}_{-0.26}$	$0.39^{+0.33}_{-0.26}$	$0.43^{+0.31}_{-0.26}$
$q_{1,TESS}$	-	$0.64^{+0.23}_{-0.30}$	$0.67^{+0.19}_{-0.16}$	0.64 ± 0.18
$q_{2,TESS}$	-	$0.36^{+0.29}_{-0.22}$	$0.24^{+0.16}_{-0.13}$	$0.20^{+0.16}_{-0.12}$
D_{TESS}	-	0.767 ± 0.036	$0.966^{+0.019}_{-0.022}$	$0.969^{+0.018}_{-0.021}$
ρ_*	kg m^{-3}	1460^{+160}_{-140}	848^{+60}_{-53}	1080^{+140}_{-110}
γ_{Blue}	m s^{-1}	-37675 ± 18	-35994 ± 9	-35999 ± 10
γ_{Red}	m s^{-1}	-37915 ± 14	-35967 ± 6	-35971 ± 6
K	m s^{-1}	243 ± 16	107.1 ± 6.2	108.0 ± 5.6
Inclination	degrees	$85.73^{+0.47}_{-0.41}$	85.21 ± 0.25	85.66 ± 0.31
a (semi-major axis)	AU	$0.04047 \pm 9.4 \cdot 10^{-4}$	0.0467 ± 0.0015	0.0467 ± 0.0015
e	-	-	-	0.346 ± 0.023
ω	degrees	-	-	$206.2^{+6.2}_{-6.7}$
M_p	M_J	1.68 ± 0.11	0.817 ± 0.047	0.773 ± 0.041
R_p	R_J	1.229 ± 0.021	1.322 ± 0.013	1.327 ± 0.014
$\ln Z$	-	5518.7	8237.3	8285.6
$\ln Z$ without a planet	-	5409.6	8104.3	-


Fig. 7. (Top) RV measurements of *Gaia*-2, on top of the best-fitting eccentric model (solid line). We subtracted the systemic velocity, listed in Table 4. (Middle) Phase-folded RV curves according to the period listed in Table 4. (Bottom) Residuals with no visible systematic variation.

Fig. 8. *Gaia*-2b: Corner plot of the posterior distribution of the main system parameters for a non-circular orbit.

photometry. For the first batch of candidates we aimed at detecting the easiest cases, i.e. hot Jupiters – giant planets that orbit their stars in short periods of a few days at most. Transiting hot Jupiters are relatively easy to detect because they exhibit relatively deep transits and the transits duty cycles are large. For the

reasons mentioned in Sect. 2, the presented search does not pretend to be exhaustive, and is far from exploiting the full detection capability of *Gaia*. We therefore do not attempt to estimate

the completeness of this search, since its statistical value is only limited at this early stage.

However, even at this point it is clear that the circumstances in the future data releases (DR4 and DR5) will allow more detections of transiting exoplanets. First, the training set used to train the classifier will be based on more data, leading to a better selection of initial candidates. More importantly, since the number of measurements in each light curve will be larger, *Gaia* photometry is bound to capture more transits, thus enhancing significantly the ability of the BLS approach to identifying them. Given the longer observation time baseline and the larger number of observations, one can predict that DR4 and DR5 will include larger sets of candidates, possibly also covering a wider range of orbital periods.

The confirmation of the two planets *Gaia*-1b and *Gaia*-2b serves to validate the presented search methodology. For *Gaia*-2b we could not rule out a more eccentric orbit, or an additional massive object that induces an RV slope, due to insufficient phase coverage, and it will probably be resolved by future RV measurements. Even without a detectable RV slope, an eccentric orbit can potentially still be the result of the presence of a third massive object in the system, which induces a non-zero eccentricity of the planet (Mazeh & Shaham 1979). In any case, even when allowing for eccentricity or an RV slope in our fits, the estimated mass of the transiting object was always less than $1.5 M_J$, well within the planetary regime.

The capability of *Gaia* to photometrically detect transiting exoplanets has often been questioned. Nevertheless, recognizing the potential, several authors have tried to estimate *Gaia* yield of transiting exoplanets (Høg 2002; Robichon, N. 2002; Dzigan & Zucker 2012), based on assumptions concerning Galactic models, planet frequency, and *Gaia* photometric performance. The *Gaia* mission has been given an indicative approval for an extension until the end of 2025⁵, probably increasing significantly the detection potential. *TESS* is performing its own all-sky survey for transiting exoplanets, but its mode of operation is focusing on short-period transits. *Gaia* is monitoring a larger sample of stars than *TESS*, and with the longer observing time span it potentially can detect long-period planets. Thus, having established that it can detect planetary transits, *Gaia* will complement the capabilities of *TESS*.

Acknowledgements. We would like to thank the anonymous referee for the insightful and helpful comments that greatly improved the analyses done in this project. This work has made use of data from the European Space Agency (ESA) mission *Gaia* (<https://www.cosmos.esa.int/gaia>), processed by the *Gaia* Data Processing and Analysis Consortium (DPAC, <https://www.cosmos.esa.int/web/gaia/dpac/consortium>). Funding for the DPAC has been provided by national institutions, some of which participate in the *Gaia* Multilateral Agreement, which include, for Switzerland, the Swiss State Secretariat for Education, Research and Innovation through the Activités Nationales Complémentaires (ANC). This work was supported by a grant from the Tel Aviv University Center for AI and Data Science (TAD) and by the Ministry of Science, Technology and Space, Israel (Grant 3-18143). This research has made use of the NASA Exoplanet Archive, which is operated by the California Institute of Technology, under contract with the National Aeronautics and Space Administration under the Exoplanet Exploration Program. We would like to thank Andrea Rossi (INAF-OAS Bologna) for carrying out the LBT observations and operating the PEPSI spectrograph. The LBT is an international collaboration among institutions in the United States, Italy and Germany. LBT Corporation partners are: The University of Arizona on behalf of the Arizona Board of Regents; Istituto Nazionale di Astrofisica, Italy; LBT Beteiligungsgesellschaft, Germany, representing the Max-Planck Society, The Leibniz Institute for Astrophysics Potsdam, and Heidelberg University; The Ohio State University, representing OSU, University of Notre Dame, University of Minnesota and University of Virginia. Python libraries used: Matplotlib (Hunter 2007), NumPy (Harris et al. 2020),

AstroPy (Astropy Collaboration et al. 2013), Lightkurve (Lightkurve Collaboration et al. 2018), juliet (Espinoza et al. 2019), batman (Kreidberg 2015), radvel (Fulton et al. 2018), dynesty (Speagle 2020), SPARTA (Shahaf et al. 2020) and Pandas (Reback et al. 2021).

References

- Akeson, R. L., Chen, X., Ciardi, D., et al. 2013, *PASP*, 125, 989–999
 Alcock, C., Allsman, R. A., Alves, D. R., et al. 2000, *ApJ*, 542, 281
 Astropy Collaboration, Robitaille, T. P., Tollerud, E. J., et al. 2013, *A&A*, 558, A33
 Borucki, W. J., Koch, D., Basri, G., et al. 2010, *Science*, 327, 977
 Bouchy, F., Udry, S., Mayor, M., et al. 2005, *A&A*, 444, L15
 Brasseur, C. E., Phillip, C., Fleming, S. W., Mullally, S. E., & White, R. L. 2019, *Astrophysics Source Code Library*, [record ascl:1905.007]
 Breiman, L. 2001, *Machine Learning*, 45, 5
 Charbonneau, D., Brown, T. M., Latham, D. W., & Mayor, M. 2000, *ApJ*, 529, L45
 Chen, T. & Guestrin, C. 2016, *ArXiv e-prints*, arXiv:1603.02754
 Dzigan, Y. & Zucker, S. 2012, *ApJ*, 753, L1
 Espinoza, N. 2018, *Res. Notes of the AAS*, 2, 209
 Espinoza, N., Brahm, R., Henning, T., et al. 2020, *MNRAS*, 491, 2982
 Espinoza, N., Kossakowski, D., & Brahm, R. 2019, *MNRAS*, 490, 2262
 Foreman-Mackey, D. 2016, *The Journal of Open Source Software*, 1, 24
 Fulton, B. J., Petigura, E. A., Blunt, S., & Sinukoff, E. 2018, *PASP*, 130, 044504
Gaia Collaboration, Prusti, T., de Bruijne, J. H. J., et al. 2016, *A&A*, 595, A1
 Harris, C. R., Millman, K. J., van der Walt, S. J., et al. 2020, *Nature*, 585, 357
 Hebb, L., Collier-Cameron, A., Triaud, A., et al. 2009, *ApJ*, 708, 224
 Hébrard, G. & Lecavelier Des Etangs, A. 2006, *A&A*, 445, 341
 Hellier, C., Anderson, D. R., Cameron, A. C., et al. 2014, *MNRAS*, 440, 1982
 Høg, E. 2002, *Astrophysics and Space Science*, 280, 139
 Holl, B., Perryman, M., Lindegren, L., Segransan, D., & Raimbault, M. 2021, *ArXiv e-prints*, arXiv:2109.02647
 Hunter, J. D. 2007, *Computing in Science Engineering*, 9, 90
 Kipping, D. M. 2013, *MNRAS*, 435, 2152
 Kovács, G., Zucker, S., & Mazeh, T. 2002, *A&A*, 391, 369
 Kreidberg, L. 2015, *PASP*, 127, 1161
 Lightkurve Collaboration, Cardoso, J. V. d. M., Hedges, C., et al. 2018, *Astrophysics Source Code Library*, [record ascl:1812.013]
 Mazeh, T. & Shaham, J. 1979, *A&A*, 77, 145
 Morton, T. D. 2015, *Astrophysics Source Code Library*, [record ascl:1503.010]
 Panahi, A. & Zucker, S. 2021, *PASP*, 133, 024502
 Perryman, M. A. C., Lindegren, L., Kovalevsky, J., et al. 1997, *A&A*, 500, 501
 Reback, J., jbrockmendel, McKinney, W., et al. 2021, *pandas-dev/pandas: Pandas 1.3.0*
 Ricker, G. R., Winn, J. N., Vanderspek, R., et al. 2015, *J. Astron. Telesc. Instrum. Syst.*, 1, 014003
 Rimoldini et al. 2022, *Gaia DR3 documentation Chapter 10: Variability*, *Gaia DR3 documentation*, European Space Agency; *Gaia Data Processing and Analysis Consortium*.
 Robichon, N. & Arenou, F. 2000, *A&A*, 355, 295
 Robichon, N. 2002, *EAS Publications Series*, 2, 215
 Shahaf, S., Binnenfeld, A., Mazeh, T., & Zucker, S. 2020, *Astrophysics Source Code Library*, [record ascl:2007.022]
 Speagle, J. S. 2020, *MNRAS*, 493, 3132
 Stassun, K. G., Oelkers, R. J., Pepper, J., et al. 2018, *AJ*, 156, 102
 Strassmeier, K. G., Ilyin, I., Järvinen, A., et al. 2015, *Astron. Nachr.*, 336, 324
 Trotta, R. 2008, *Contemporary Physics*, 49, 71
 Wu, Y. 2003, *ASP Conf. Ser.*, 294, 213
 Zechmeister, M. & Kürster, M. 2009, *A&A*, 496, 577
 Zucker, S. 2003, *MNRAS*, 342, 1291

⁵ <https://sci.esa.int/web/director-desk/-/extended-options-confirmed-for-science-missions>